Nanoscale

PAPER

View Article Online
View Journal | View Issue

Cite this: *Nanoscale*, 2014, **6**, 9443

Geometric nonlinearity and mechanical anisotropy in strained helical nanoribbons

Z. Chen

Received 18th January 2014
Accepted 4th April 2014

DOI: 10.1039/c4nr00336e

www.rsc.org/nanoscale

Fabrication and synthesis of helical nanoribbons have received increasing attention because of the broad applications of helical nanostructures in nano-elecromechanical/micro-electromechanical systems (NEMS/MEMS), sensors, active materials, drug delivery, *etc.* In this paper, I study the mechanical principles used in designing strained helical nanoribbons, and propose the use of a full three-dimensional finite element method to simulate the coexistence of both left- and right-handed segments in the same strained nanoribbon. This work can both help understand the large deformation behaviours of such nanostructures and assist in the design of helical nanostructures for engineering applications.

1 Introduction

Helical structures are among the most universal shapes in nature and engineering materials.[1] Helical shapes are found in many natural systems, including DNA,[2] chiral seed pods,[3] tendrils of plants,[4–6] *etc.* Mechanical self-assembly of helical structures has received continuous attention from the research community because of its potential applications in nano-elecromechanical/micro-electromechanical systems (NEMS/MEMS), sensors,[7] microrobotics,[8] active materials,[9] drug delivery,[10] and optoelectronics.[11]

Helical ribbon shapes often result from the competition between bending and stretching energies, as well as due to a variety of driving forces,[3,12–22] including, but not limited to, surface stresses,[12–15] residual stresses,[5,16] misfit strains,[18–21] piezoelectricity,[22] differential growth,[23,24] and swelling/de-swelling.[3,25] The transition between different helical shapes, for instance, the purely twisted and nearly cylindrical helical shapes, can occur due to the complex interplay between the molecular interactions, chiral twists, and ribbon elasticity.[26–30] While the selection of shapes typically relies on the detailed mechanisms involved in an individual system,[26–33] some common features exist, *e.g.* the kinematics involved in such geometrical changes stay the same.[10,11]

In strained helical nanoribbons, the main driving force is the misfit strain between different layers. A remarkable feature in such "nanomechanical architectures" is the versatile combination of materials that can be used.[34–39] Although the analytic solution exists for predicting the rolling radius in such strained nanostructures, more complex behaviours, such as the co-existence of both left- and right-handed components,[18] the change of chirality,[5,16,18,19,37] and multistability,[40–49] still remain to be explored.

Noticeably, Zhang *et al.*[19] reported the anomalous coiling behaviours in SiGe/Si and SiGe/Si/Cr nanohelices. Specifically, as the width decreases from 1.3 μm to 0.7 μm, the pitch and helix angle of the SiGe/Si/Cr helical nanobelt first decrease, then increase, and finally decrease until a self-overlapping multi-turn ring is formed when the width is reduced to 0.7 μm. During this process, the chirality also changes from right-handed to mixed and to left-handed, in addition to the variance of pitch, helix angle and geometric orientation. To interpret this novel phenomenon, Zhang *et al.* considered the edge effects and hypothesized that the edge stress will become increasingly dominating, resulting in the change of chirality, and the eventual self-overlapping ring shape when the ribbon width falls below a threshold.[19] Dai and Shen further employed Cosserat rod theory to explain the mechanical mechanism by again considering the rising edge effects as the width decreases.[36] Not only can the chirality of strained semiconductor nanohelices change under certain circumstances, but there can also exist helical nanoribbons with co-existing left-handed and right-handed segments. These helical nano-structures have important applications in micro-capacitors, inductors,[18] and motion converters.[37] Interestingly, when there is self-contact, a shape transition into a tightly coiled helical structure with only one handedness can occur.[17]

In this work, I study the mechanical principles involved in designing strained helical nanoribbons, in particular, principles related to engineering the pitch, radius, orientation and chirality of helical nanoribbons. Furthermore, a finite element method is used to simulate the spontaneous deformation of strained nanoribbons with both left-handed and right-handed segments. This work can promote understanding of the mechanical self-assembly principle of three-dimensional chiral structures, and aid the programmable design and manufacturing of spontaneously helical nanostructures for NEMS and MEMS applications.

Department of Biomedical Engineering, Washington University, St. Louis 63130, USA. E-mail: zichen@alumni.princeton.edu

2 Results and discussion

Helical ribbon shapes often result from anisotropic mechanical stresses and geometric misalignment between the principal axes of the driving force and the geometric axes of the ribbon (*i.e.*, the length and width directions).[12,13] Previous studies[12,13] have shown that four independent parameters, κ_1, κ_2, Φ and w control the shape of a helical ribbon (where Φ is the misorientation angle and w is the width of the ribbon). A purely twisted ribbon (Fig. 1a) forms when $\kappa_1 \cos^2 \Phi + \kappa_2 \sin^2 \Phi = 0$ (with a negative Gaussian curvature, *i.e.*, $\kappa_G < 0$); when either κ_1 or κ_2 vanishes ($\kappa_G = 0$), the ribbon forms a cylindrical helical ribbon; when $\kappa_G > 0$, a general helical ribbon with a concave surface results (Fig. 1c). Moreover, recent studies have shown that geometric nonlinearity can give rise to selection of shape and multi-stability in helical ribbons.[33]

To study the anomalous coiling of nanoribbons, I noticed that in Zhang *et al.*'s study[19] the width around which the SiGe/Si/Cr nanobelt switches shape from a helical ribbon to a ring shape is 0.8 μm or 0.7 μm.[19] The corresponding value of the dimensionless parameter, $\eta = w\sqrt{k/h}$,[3,15] is around 3.27 or 2.85, in the same order of magnitude as the critical value $\eta_c = \sqrt[4]{80(1+\nu)/3} \approx 2.4$. Therefore, it is worth investigating whether geometric nonlinearity plays a role in the anomalous coiling of these strained helical ribbons. Taking into account the nonlinear geometric effects (competition between the bending and stretching energy), the ribbon, when subjected to an equal biaxial misfit strain, adopts a ring shape.[12,13] This result is consistent with the experimental observation in SiGe/Si/Cr nanobelts. The value of η at which the change of chirality occurs ($w = 1.1$ μm) is calculated to be $4.5 \gg \eta_c$, so the ribbon is still in the regime ($\eta \gg \eta_c$) where it should form a nearly cylindrical helical shape because of geometric nonlinearity.

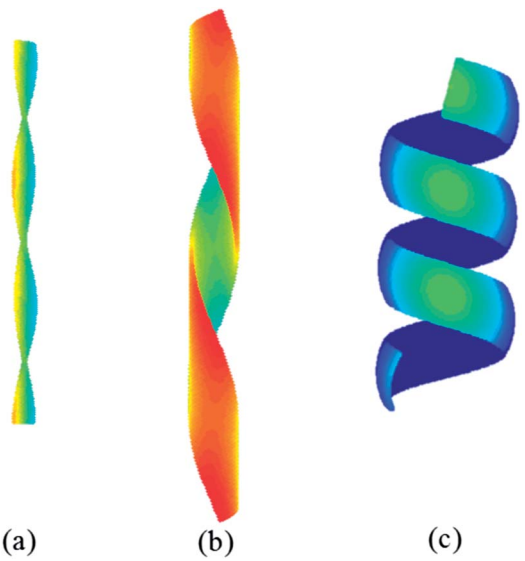

Fig. 1 Helical ribbon shapes with different Gaussian curvatures. $\kappa_G = \kappa_1\kappa_2$, where κ_1 and κ_2 are the principal curvatures. (a) $\kappa_G < 0$; (b) $\kappa_G = 0$; (c) $\kappa_G > 0$.

Moreover, due to nonlinear geometric effects,[3,15] bistable behaviors can occur resulting in the change of helical pitch, radius and orientation.[33] While there are similar characteristics between the shape transition of bistable helical ribbons and the anomalous coiling of strained helical nanoribbons, there is no change in chirality in the previous phenomena. Therefore, geometric nonlinearity may not be the main reason for the anomalous coiling, instead, the increasingly significant edge stresses (when the width decreases) are the main cause for such behaviors, as previously hypothesized by the researchers. In fact, this principle can be employed to design and manufacture nanostructures with applications in MEMS/NEMS.

Nevertheless, the geometric nonlinearity can still play an important role in generating cylindrical helical ribbons in a lot of cases, and can possibly be exploited in designing multistable strained semiconductor structures. The interaction between geometric nonlinear effects and mechanical anisotropy in crystalline materials remains to be explored.

Here, it is worth noting that the existence of mechanical anisotropy due to preferred rolling along the most compliant direction adds another dimension to the designing of helical nanostructures. Along with this type of mechanical anisotropy comes the difficulty in modeling spontaneous deformation due to lattice mismatch. In this work, this difficulty is overcome by assuming the material properties to be isotropic and linear elastic, while suppressing the misfit strain along the direction perpendicular to the most compliant bending direction. By so doing, similar deformation can be achieved as compared to the mechanically anisotropic system of interest.

For a bilayer strained heterostructure[38] (Fig. 2), the radius is determined analytically as $R = (h_1^4 + 4\alpha h_1^3 h_2 + 6\alpha h_1^2 h_2^2 + 4\alpha h_1 h_2^3 + \alpha^2 h_2^4)/[6\varepsilon_0\alpha(1+\nu)h_1h_2(h_1+h_2)]$. Here, since $R \sim h/\varepsilon_0$, it is convenient to simulate the large deformation using the set of parameters $(a\varepsilon_0, ah_1, ah_2)$ instead of $(\varepsilon_0, h_1, h_2)$ for an arbitrary value of a. This can be useful when the numerical issue emerges as the thickness becomes too small (in the nanoscale).

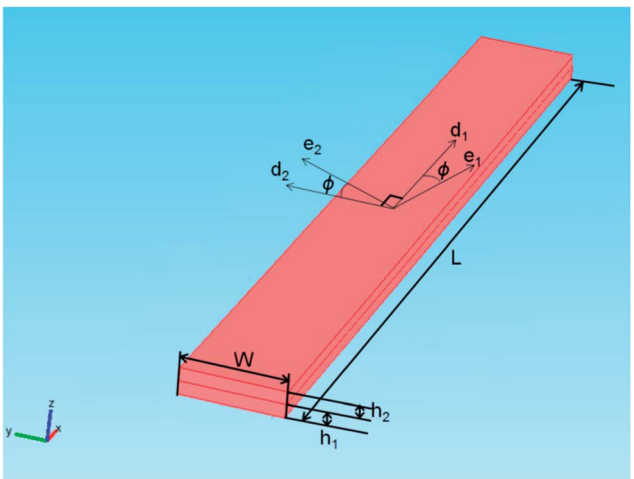

Fig. 2 Geometry of a bilayer strained nanoribbon before releasing from the substrate.

While the analytical solution exists for the simplest case where the strained nanoribbon adopts a cylindrical (helical) shape and Poisson's ratio is constant throughout multiple layers, there are scenarios where such solution may not exist. For example, there could be co-existing left-handed and right-handed segments in SiGe/Si/Cr nanobelts where the misalignment angle is slightly larger than 45 degrees and the tip has an influence on the preferred chirality.[18,37] While qualitative interpretation of such behaviour was provided, quantitative modelling remains a challenge. To this end, I employ a finite element method[20,49] to simulate this process (Fig. 3). A strained nanoribbon of length $L = 3.2$ μm, width $w = 0.1$ μm, thickness $h_1 = h_2 = 5$ nm, and misfit strain $\varepsilon_0 = 0.05$ is divided into two connecting segments of length 0.8 μm and 2.4 μm, respectively. The misalignment angle (between the ribbon's long axis and the preferred bending axis <100>) in the lower segment ribbon is 50 degrees, and the misalignment angle in the upper segment is also 50 degrees. The deformed shape exhibits co-existence of both left- and right-handed parts connected by a perversion,[5,16,18] consistent with the experimental result by Zhang *et al.*[18] (inset of Fig. 3). Here, it is worth mentioning that it is important to incorporate geometric nonlinearity in the finite element simulations.

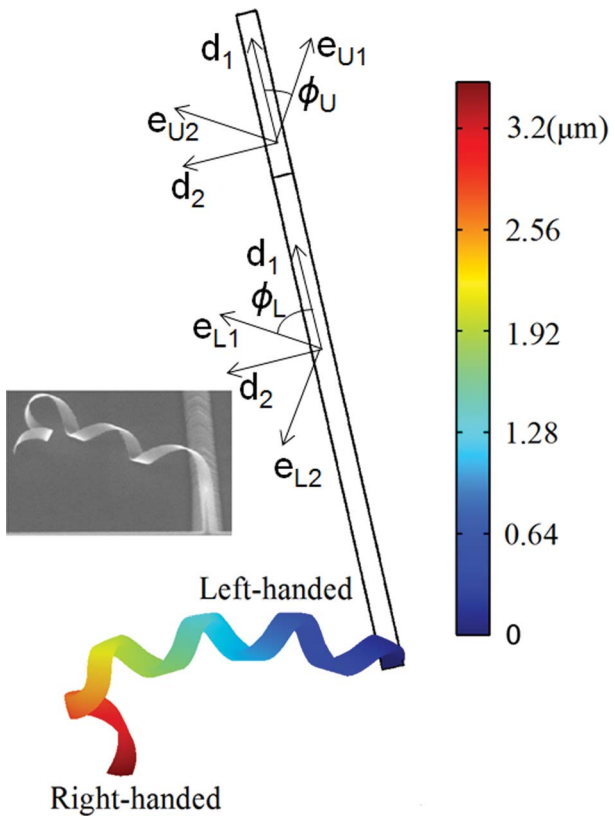

Fig. 3 A helical nanoribbon with both left-handed and right-handed segments with only one fixed end. Here, $\Phi_L = 50°$, $\Phi_U = 40°$ and $\varepsilon_0 = 0.05$. In the upper segment (of length 0.8 μm), the effective misfit strain tensor of the bottom layer is $\varepsilon_b = \varepsilon_0 e_{U2} \otimes e_{U2}$. In the lower segment (of length 2.4 μm), the effective misfit strain tensor of the bottom layer is $\varepsilon_b = \varepsilon_0 e_{L2} \otimes e_{L2}$. Inset: (adapted from Fig. 7 by Zhang *et al.*[18]). The color indicates the total displacement.

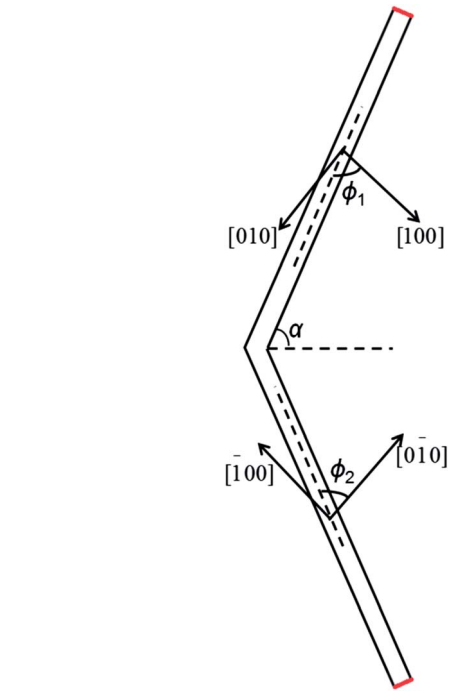

Fig. 4 Geometry of a symmetric mesa design. Both ends (in red) are fixed.

I also use this framework to study the spontaneous deformation of a V-shaped mesa design.[18] Fig. 4 shows the geometric parameter involved in such a mesa shape. It can be shown that the angles satisfy the geometric relationship: $2\alpha + \Phi_1 + \Phi_2 = 270°$. In order to develop symmetric left- and right-handed

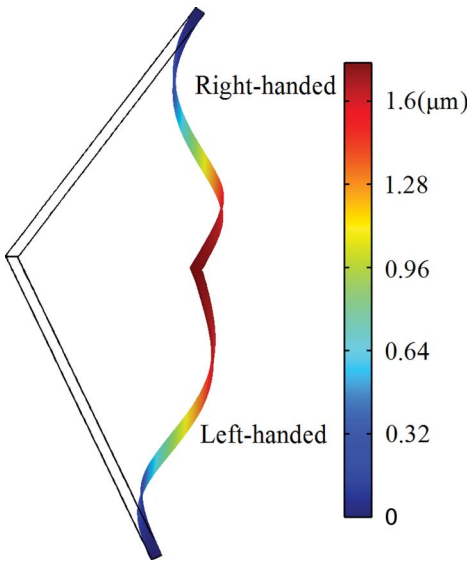

Fig. 5 A strained nanoribbon with symmetric left-handed and right-handed segments (both ends being fixed). Here, $\Phi_1 = \Phi_2 = 75°$, $\varepsilon_0 = 0.024$. In the upper segment, the effective misfit strain tensor of the bottom layer is $\varepsilon_b = \varepsilon_0 e_{U1} \otimes e_{U1}$, where $e_{U1} = [100]$ and $e_{U2} = [010]$. In the lower segment, the effective misfit strain tensor of the bottom layer is $\varepsilon_b = \varepsilon_0 e_{L1} \otimes e_{L1}$, where $e_{L1} = [0\bar{1}0]$ and $e_{L2} = [\bar{1}00]$. The color indicates the total displacement.

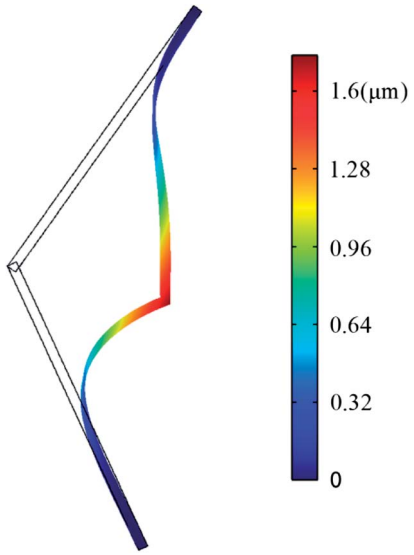

Fig. 6 A strained nanoribbon with asymmetric left-handed and right-handed segments (both ends being fixed). Here, $\Phi_1 = 86°$, $\Phi_2 = 64°$; $\varepsilon_0 = 0.01$. In the upper segment, the effective misfit strain tensor of the bottom layer is $\varepsilon_b = \varepsilon_0 e_{U1} \otimes e_{U1}$, where $e_{U1} = [100]$ and $e_{U2} = [010]$. In the lower segment, the effective misfit strain tensor of the bottom layer is $\varepsilon_b = \varepsilon_0 e_{L1} \otimes e_{L1}$, where $e_{L1} = [0\bar{1}0]$ and $e_{L2} = [\bar{1}00]$. The color indicates the total displacement.

helical shapes, Φ_1 should be equal to Φ_2. An example is given in Fig. 5, where $\Phi_1 = \Phi_2 = 75°$ and $\alpha = 60°$.

Yet another example of the application of the current methodology is the design of asymmetric helical shapes with both left- and right-handed components. This can be achieved by assuming $\Phi_1 \neq \Phi_2$. In Fig. 6, for instance, $\Phi_1 = 86°$, $\Phi_2 = 64°$, when $\alpha = 60°$. The resulting shape is similar in nature to the helical nanostructure developed by Zhang *et al.*[18]

3 Finite element simulations

The finite element model used in this work is a full three-dimensional model that uses the structural mechanics module of Comsol Multiphysics V4.3a with the methodology detailed in ref. 20 and 49. This model was employed to study the shape transition and multi-stability in helical ribbon structures driven by misfit or residual strains between different layers in an initially flat elastic ribbon.[3,12,13,19] Young's modulus of Si is 168.9 GPa and that of SiGe is 161.2 GPa.[35] Poisson's ratio of both layers is 0.27.[36]

4 Conclusions

In this work, the mechanical principles involved in designing helical nanoribbons through strain engineering were explored. The possibility of exploiting geometric nonlinearity and mechanical anisotropy to shape strained helical nanoribbons was also discussed. Furthermore, three-dimensional finite element simulations were employed to study the more complicated cases where both left-handed and right-handed components exist in one ribbon, with either one end or both ends fixed. The results of this study can complement the recent theoretical, experimental and computational studies on the mechanical self-assembly of spontaneous helical structures and multi-stable structures, and will promote quantitative understanding of engineering shapes in these nanostructures. This work can also facilitate the programmable design of functional nanostructures with a variety of potential applications in NEMS/MEMS, sensors, drug delivery, active materials, optoelectronics, and bio-inspired robotics.

Acknowledgements

Z.C. is supported by Society in Science, The Branco Weiss Fellowship, administered by ETH Zurich.

Notes and references

1 N. Chouaieb, A. Goriely and J. H. Maddocks, *Proc. Natl. Acad. Sci. U. S. A.*, 2006, **103**, 9398–9403.
2 Y. Y. Biton, B. D. Coleman and D. Swigon, *J. Elastomers Plast.*, 2007, **87**, 187–210.
3 S. Armon, E. Efrati, R. Kupferman and E. Sharon, *Science*, 2011, **333**, 1726–1730.
4 A. Goriely and M. Tabor, *Phys. Rev. Lett.*, 1998, **80**, 1564–1568.
5 S. J. Gerbode, J. R. Puzey, A. G. McCormick and L. Mahadevan, *Science*, 2012, **337**, 1087–1091.
6 J. Wang, G. Wang, X. Feng, T. Kitamura, Y. Kang, S. Yu and Q. Qin, *Sci. Rep.*, 2013, **3**, 3102.
7 Y. Sawa, K. Urayama, T. Takigawa, V. Gimnez-Pinto, B. L. Mbanga, F. Ye, J. V. Selinger and R. L. B. Selinger, *Phys. Rev. E: Stat., Nonlinear, Soft Matter Phys.*, 2013, **88**, 022502.
8 J. J. Abbott, K. E. Peyer, M. C. Lagomarsino, L. Zhang, L. X. Dong, I. K. Kaliakatsos and B. J. Nelson, *Int. J. Robot. Res.*, 2009, **28**, 1434–1447.
9 Q. Ge, H. J. Qi and M. L. Dunn, *Appl. Phys. Lett.*, 2013, **103**, 131901.
10 I. W. Hamley, A. Dehsorkhi, V. Castelletto, S. Furzeland, D. Atkins, J. Seitsonen and J. Ruokolainen, *Soft Matter*, 2013, **9**, 9290–9293.
11 G. Hwang, C. Dockendorf, D. Bell, L. Dong, H. Hashimoto, D. Poulikakos and B. Nelson, *Int. J. Optomechatronics*, 2008, **2**, 88–103.
12 Z. Chen, C. Majidi, D. J. Srolovitz and M. Haataja, *Appl. Phys. Lett.*, 2011, **98**, 011906.
13 Z. Chen, C. Majidi, D. J. Srolovitz and M. Haataja, 2012, arXiv:1209.3321.
14 J. Wang, X. Feng, G. Wang and S. Yu, *Appl. Phys. Lett.*, 2008, **92**, 191901.
15 Z. Chen, Q. Guo, C. Majidi, W. Chen, D. J. Srolovitz and M. Haataja, *Phys. Rev. Lett.*, 2012, **109**, 114302.
16 J. Huang, J. Liu, B. Kroll, K. Bertoldi and D. R. Clarke, *Soft Matter*, 2012, **8**, 6291–6300.
17 Q. Guo, Z. Chen, W. Li, P. Dai, K. Ren, J. Lin, L. A. Taber and W. Chen, *EPL*, 2014, **105**, 64005.
18 L. Zhang, E. Deckhardt, A. Weber, C. Schönenberger and D. Grützmacher, *Nanotechnology*, 2005, **16**, 655.

19 L. Zhang, E. Ruh, D. Grützmacher, L. Dong, D. J. Bell, B. J. Nelson and C. Schönenberger, *Nano Lett.*, 2006, **6**, 1311–1317.
20 Q. Guo, H. Zheng, W. Chen and Z. Chen, *J. Mech. Med. Biol.*, 2013, **13**, 1340018.
21 Z. Suo, E. Y. Ma, H. Gleskova and S. Wagner, *Appl. Phys. Lett.*, 1999, **74**, 1177–1179.
22 C. Majidi, Z. Chen, D. J. Srolovitz and M. Haataja, *J. Mech. Phys. Solids*, 2010, **58**, 73–85.
23 T. Savin, N. A. Kurpios, A. E. Shyer, P. Florescu, H. Liang, L. Mahadevan and C. J. Tabin, *Nature*, 2011, **476**, 57–62.
24 M. A. Wyczalkowski, Z. Chen, B. A. Filas, V. D. Varner and L. A. Taber, *Birth Defects Res., Part C*, 2012, **96**, 132–152.
25 W. Li, G. Huang, H. Yan, J. Wang, Y. Yu, X. Hu, X. Wu and Y. Mei, *Soft Matter*, 2012, **8**, 7103–7107.
26 Y. Sawa, F. Ye, K. Urayama, T. Takigawa, V. Gimenez-Pinto, R. L. B. Selinger and J. V. Selinger, *Proc. Natl. Acad. Sci. U. S. A.*, 2011, **108**, 6364–6368.
27 J. V. Selinger, M. S. Spector and J. M. Schnur, *J. Phys. Chem. B*, 2001, **105**, 7157–7169.
28 R. Oda, I. Huc, M. Schmutz, S. J. Candau and F. C. MacKintosh, *Nature*, 1999, **399**, 566–569.
29 L. Teresi and V. Varano, *Soft Matter*, 2013, **9**, 3081–3088.
30 T. Gibaud, E. Barry, M. J. Zakhary, M. Henglin, A. Ward, Y. Yang, C. Berciu, R. Oldenbourg, M. F. Hagan, D. Nicastro, R. B. Meyer and Z. Dogic, *Nature*, 2012, **481**, 348–351.
31 W. S. Childers, N. R. Anthony, A. K. Mehta, K. M. Berland and D. G. Lynn, *Langmuir*, 2012, **28**, 6386–6395.
32 G. Bellesia, M. V. Fedorov and E. G. Timoshenko, *J. Chem. Phys.*, 2008, **128**, 195105.
33 Q. Guo, A. K. Mehta, M. A. Grover, W. Chen, D. G. Lynn and Z. Chen, *Appl. Phys. Lett.*, arXiv:1312.3571., in press
34 M. Huang, C. Boone, M. Roberts, D. E. Savage, M. G. Lagally, N. Shaji, H. Qin, R. Blick, J. A. Nairn and F. Liu, *Adv. Mater.*, 2005, **17**, 2860–2864.
35 (*a*) M. Huang, F. Cavallo, F. Liu and M. G. Lagally, *Nanoscale*, 2011, **3**, 96–120; (*b*) L. Dai and L. Zhang, *Nanoscale*, 2013, **5**, 971–976.
36 L. Dai and W. Z. Shen, *J. Appl. Phys.*, 2009, **106**, 114314.
37 L. Dong, L. Zhang, B. E. Kratochvil, K. Shou and B. J. Nelson, *J. Microelectromech. Syst.*, 2009, **18**, 1047–1053.
38 M. Grundmann, *Appl. Phys. Lett.*, 2003, **83**, 2444–2446.
39 P. Froeter, X. Yu, W. Huang, F. Du, M. Li, I. Chun, S. H. Kim, K. J. Hsia, J. A. Rogers and X. Li, *Nanotechnology*, 2013, **24**, 475301.
40 R. Ghafouri and R. Bruinsma, *Phys. Rev. Lett.*, 2005, **94**, 138101.
41 E. Kebadze, S. D. Guest and S. Pellegrino, *Int. J. Solids Struct.*, 2004, **41**, 2801–2820.
42 S. Daynes, C. G. Diaconu, K. D. Potter and P. M. Weaver, *J. Compos. Mater.*, 2010, **44**, 1119–1137.
43 S. Vidoli and C. Maurini, *Proc. R. Soc. A*, 2008, **464**, 2949–2966.
44 X. Lachenal, P. M. Weaver and S. Daynes, *Proc. R. Soc. A*, 2012, **468**, 1230–1251.
45 Y. Forterre, J. M. Skothelm, J. Dumais and L. Mahadevan, *Nature*, 2005, **433**, 421–425.
46 H. Zheng, Y. Liu and Z. Chen, *Journal of Postdoctoral Research*, 2013, **1**, 40–50.
47 M. Shahinpoor, *Bioinspiration Biomimetics*, 2011, **6**, 046004.
48 F. Arrieta, P. Hagedorn, A. Erturk and D. J. Inman, *Appl. Phys. Lett.*, 2010, **97**, 104102.
49 Q. Guo, H. Zheng, W. Chen and Z. Chen, *Bio-Med. Mater. Eng.*, 2014, **24**, 557–562.